NeuroImage xxx (2009) xxx–xxx

Contents lists available at ScienceDirect

NeuroImage

journal homepage: www.elsevier.com/locate/ynimg

White matter architecture rather than cortical surface area correlates with the EEG alpha rhythm

Pedro A. Valdés-Hernández *,[1], Alejandro Ojeda-Gonzalez [1], Eduardo Martinez-Montes, Agustín Lage-Castellanos, Trinidad Virués-Alba, Lourdes Valdés-Urrutia, Pedro A. Valdés-Sosa

Neuroimaging Department, Cuban Neuroscience Center, Ave 25, Esq. 158, #15202, PO Box 6412/6414, Cubanacán, Playa, Havana, Cuba

ARTICLE INFO

Article history:
Received 18 June 2009
Revised 8 October 2009
Accepted 10 October 2009
Available online xxxx

ABSTRACT

There are few studies on the neuroanatomical determinants of EEG spectral properties that would explain its substantial inter-individual variability in spite of decades of biophysical modeling that predicts this type of relationship. An exception is the negative relation between head size and the spectral position of the alpha peak (P_α) reported in Nunez et al. (1978)—proposed as evidence of the influence of global boundary conditions on slightly damped neocortical waves. Here, we attempt to reexamine this finding by computing the correlations of occipital P_α with various measures of head size and cortical surface area, for 222 subjects from the EEG/MRI database of the Cuban Human Brain Mapping Project. No relation is found ($p>0.05$). On the other hand, biophysical models also predict that white matter architecture, determining time delays and connectivities, could have an important influence on P_α. This led us to explore relations between P_α and DTI fractional anisotropy by means of a multivariate penalized regression. Clusters of voxels with highly significant relations were found. These were positive within the Posterior and Superior Corona Radiata for both hemispheres, supporting biophysical theories predicting that the period of cortico-thalamocortical cycles might be modulating the alpha frequency. Posterior commissural fibers of the Corpus Callosum present the strongest relationships, negative in the inferior part (Splenium), connecting the inferior occipital lobes and positive in the superior part (Isthmus and Tapetum), connecting the superior occipital cortices. We found that white matter architecture rather than neocortical area determines the dynamics of the alpha rhythm.

Introduction

In the past, detailed biophysical models have been proposed for the generation of EEG rhythms (David and Friston, 2003; Izhikevich and Edelman, 2008; Niedermeyer and Lopes da Silva, 2004; Nunez et al., 1995; Robinson et al., 2003a; Valdes-Sosa et al., in press)—all depending on neuroanatomical-based parameters. It is therefore surprising that there are few experimental attempts to explain the considerable inter-subject variability of the EEG on the basis of measured individual neuroanatomical characteristics. We aim in this paper to provide additional insights into this issue by reviewing some of the previous results as well as providing novel findings. Understanding such relationships would not only contribute to the knowledge about the genesis of the electrophysiological phenomena but would also allow the elimination of uncontrolled sources of variance that decrease the sensitivity of experimental or clinical studies on individual subjects.

One important empirical work, exploring the neuroanatomical basis of EEG during maturation is that of Whitford et al. (2007), where decreases of EEG power, especially in the slow-wave band, mirrored gray matter volume decreases from 10 to 30 years. This was directly confirmed by a significant regression between these two variables. They did not report significant relations between white matter volume and EEG power and concluded that a reduction of the neuropil, reflected in gray matter volume decreases, would correspond to the elimination of active synapses causing concurrent EEG power reduction.

Our concern in this paper is not with changes of *power* within specific EEG bands but rather of a distinctive signature of the normal resting human EEG, the spectral position of the alpha peak or *the alpha frequency* (P_α). Among the quantitative EEG parameters, P_α is the best signature of maturation (Valdés et al., 1990); the EEG feature with the highest heritability (Posthuma et al., 2001); and a sensitive indicator of pathology (Valdes et al., 1992). Exploration of the neuroanatomical determinants of P_α compels us to the examination of the theories about the generation of the alpha rhythm. This has been the subject of several biophysical models which could be classified according to the neuroanatomical scales and structures involved: (i) *pacemakers*, (ii) *local* and (iii) *global* and (iv) *local-global*

* Corresponding author. Fax: +53 7 208 6707.
E-mail address: multivac@cneuro.edu.cu (P.A. Valdés-Hernández).
[1] Asterisk indicates equal contributions.

1053-8119/$ – see front matter © 2009 Published by Elsevier Inc.
doi:10.1016/j.neuroimage.2009.10.030

combinations. From another point of view, they can also be classified as (a) *thalamic*, (b) *cortical* or (c) *thalamic-cortical*.

The *pacemaker theory* is supported by the intrinsic oscillation properties of some neural cells, e.g. those in the thalamus (Andersen and Andersson, 1968; Jahnsen and Llinas, 1984) or pyramidal cells in layer V of the neocortex (Bollimunta et al., 2008; Connors and Amitai, 1997; Flint and Connors, 1996; Lopes da Silva, 1991). This theory is unable to explain most of the global EEG phenomena, e.g. the relative frequencies of major rhythms and sleep-wave variations (Robinson et al., 2001b). However, the intrinsic oscillatory behavior of those cells may probably shape the rhythmic behavior of networks to which they belong (Lopes da Silva, 1991).

The *local models* of alpha oscillations comprise excitatory and inhibitory populations of neurons interacting via dendritic response functions and nonlinearities. These two populations can be the thalamocortical relay and reticular neurons in the thalamus (Lopes da Silva et al., 1974) or the pyramidal cells and interneurons in the cortex. A local cortical model is described in Van Rotterdam et al. (1982), where a chain of cortical excitatory–inhibitory modules predicted intracortical alpha waves with speed of 30 cm/s, in agreement with the experimental finding in (Lopes da Silva and Storm van Leeuwen, 1978). Other local models deal with the dynamics of either a single (Jansen et al., 1993) or coupled cortical columns (Jansen and Rit, 1995), although these two have been criticized in Grimbert and Faugeras (2006) for being unable to reproduce alpha rhythm across the whole range of possible physiological parameters in the model. In general, the local models, although contributing to the global dynamics of the global alpha rhythm, do not account for the significant spatial coherence, within the alpha band, between distant scalp areas, reported in the literature (Cantero et al., 1999; Niedermeyer and Lopes da Silva, 2004; Nunez et al., 2001).

On the other hand, large-scale networks of connected neuronal populations can generate the global alpha rhythm, as predicted by Izhikevich and Edelman (2008), Liley et al. (1999), Liley et al. (2002), Nunez et al. (1995), Sotero et al. (2007), Valdes-Sosa et al. (in press), and Wright et al. (2001). In particular, purely *global models* ignore dendritic response functions and finite intracortical propagation thus depending on propagation delays between distant anatomical structures only. The paradigmatic example of this type of modeling is Nunez et al. (1995) for the generation of the human alpha rhythm. This model is *cortical* based on the argument that only 1% of cortical input to the human brain is from the thalamus, the rest consisting of cortico-cortical connections. In this model, the boundary conditions affects spectral properties of the EEG rhythms, leading to the *cortical standing wave theory of the EEG*, recently reviewed in Nunez and Srinivasan (2006), which, to our knowledge, is the only global model that has been subjected to empirical tests. A *traveling wave* behavior of electrical activity through the neocortex was also suggested by Nunez et al. (1978). There is evidence for this in experimental reports and reviews, based on scalp EEG (Burkitt et al., 2000; Hughes et al., 1992; Hughes et al., 1995; Lopes da Silva, 1991; Manjarrez et al., 2007; Massimini et al., 2004; Wingeier et al., 2001). Moreover, these waves were recently measured directly with optical imaging in Wu et al. (2008). In Nunez et al. (1995), traveling waves are predicted to be slightly damped. Since the neocortex is a closed 2D surface, these waves might interfere to form standing waves. Some patterns of scalp EEG for visual evoked steady-states, presented in Chapter 6 of Nunez et al. (1995), seem to support this hypothesis. According to this theory, the eigenfrequencies of the standing waves are equal to those of the EEG rhythms. The boundary conditions of this system are determined by *neocortical surface area* (NSA) which is predicted to be inversely proportional to the eigenfrequencies (Nunez et al., 1995).

The cortical standing wave theory has been criticized by Rennie et al. (1999), Robinson et al. (1997, 2001a) and Wright and Liley (1996) who suggested that the high damping rates of cortical traveling waves preclude boundary condition affecting the dynamical properties of the alpha rhythm. Such high damping rates must produce excessively blurred peak resonances in contrast with observations (Robinson et al., 2001b), even though Robinson et al. (2001b) predicted a decrease of damping due to thalamocortical resonances. To date, there is no strong experimental evidence for "standing waves" on the neocortex. There is only an indirect verification in Nunez et al. (1978) where a mild negative correlation between head size and the P_α is reported, a result replicated by Posthuma et al. (2001). Nunez et al. (1978) used head size as a proxy for NSA due to the unavailability, at that time, of suitable techniques to measure *in vivo* the latter in individuals. With the availability of current Neuroimaging and Neuroinformatics tools (Ashburner and Friston, 1999; Mazziotta et al., 2001; Robbins, 2003; Smith, 2002), the relation between NSA and the P_α may now be reexamined by using direct measurement of NSA in a large sample of individuals. This would provide stronger support or falsification for the actual existence of EEG neocortical standing waves. This experimental test is one of the prime objectives of this paper.

On the other hand, there are many models in the literature with *combinations* of *global and local features*. The inclusion of local features results in waves that are more damped than those of the "EEG cortical standing waves theory," and therefore minimizes the effects of boundaries (Robinson et al., 2001b; Wright and Liley, 1996). These models can be cortical (Jirsa and Haken, 1997; Liley et al., 1999; Liley et al., 2002; Nunez et al., 1995; Robinson et al., 1998; Wright and Liley, 1995) or thalamic-cortical (Robinson et al., 2001c, 2003a), depending on the importance given to the thalamus in the generation of the alpha rhythm. Nevertheless, the role of thalamocortical, corticothalamic and corticocortical interactions appears to be determinant in the generation of the alpha rhythm, as experimentally suggested in Lopes da Silva et al. (1980), for the dog, with the method known as "theoretical thalamic deafferentation," which consists in computing partial coherence functions. In fact, the thalamic-cortical model treated in Robinson et al. (2003a), strikingly predicts the spectral characteristic of the alpha rhythm, e.g. the peak width not predicted by the "EEG cortical standing wave theory," in addition to other EEG phenomena such as the topographical distribution of the alpha splitting (Robinson et al., 2003b).

Current Neuroimaging techniques allow the *in vivo* examination of other neuroanatomical determinants of the P_α. The principal ingredient added to large-scale models (global, global-local, cortical or thalamic-cortical) is the long range connections via white matter. Therefore, most relevant would be the neuroanatomical correlates of axonal *connectivities* and *time delays* in thalamocortical, corticothalamic and corticocortical circuitries. For example, connectivity strength theoretically is related to the frequency of coupled cortical areas (David and Friston, 2003; Sotero et al., 2007). Time delays appear to be even more important (David and Friston, 2003; Jirsa, 2009; Jirsa and Haken, 1997; Robinson et al., 2003a,b; Valdes-Sosa et al., in press). In fact, in the general equations governing the "EEG cortical wave theory" (Nunez et al., 1995; Nunez and Srinivasan, 2006), the eigenfrequencies depend more on time delays in long range corticocortical axons than on NSA. In particular, a theoretical prediction that strengthens the role of the thalamus in the generation of the alpha rhythm is that of Roberts and Robinson (2008) and Robinson et al. (2001b) where P_α is found to be most sensitive, and inversely proportional, to the period of corticothalamic feedback.

In the conduction, along the bundles of axons connecting two different gray matter regions, the strength of the connectivity is roughly determined by the number of axons (Iturria-Medina et al., 2007) and therefore depends on *fiber density*, i.e. the number of fibers per unit of cross-sectional area whereas time delay is determined by conduction velocity which depends on *myelination* (Sabah, 2000), i.e. the cross-sectional area occupied by myelin sheath as well as, possibly, on *fiber density* (Reutskiy et al., 2003). Both fiber density and myelination can be quantified locally with Neuroimaging. All the

Please cite this article as: Valdés-Hernández, P.A., et al., White matter architecture rather than cortical surface area correlates with the EEG alpha rhythm, NeuroImage (2009), doi:10.1016/j.neuroimage.2009.10.030

above theoretical work strongly encourages exploring, firstly at the phenomenological level, the relation of these neuroanatomical parameters with P_α.

The Image of Diffusion Tensor Fractional Anisotropy (FA) is a suitable candidate for the *in vivo* characterization of fiber density and myelination. This is an average-in-a-voxel measure of the anisotropic profile of water motion in a heterogeneous medium that can be easily measured nowadays with MRI. For the particular case of a *single bundle of parallel axons*, FA is theoretically directly proportional to the fraction of cross-sectional area occupied by the axons in the extracellular space (Hwang et al., 2003; Pabitra and Basser, 2005) (see Appendix A) and precisely this fraction is directly proportional to fiber density and myelination. Indeed, the experimental evidence of the effect of fiber density on FA is reviewed in Beaulieu (2002) and Le Bihan (2007). Moreover, FA within certain white matter tracts of the brain has been recently found to be significantly predicted by White Matter Fraction Images in a linear model with positive slope (Mädler et al., 2008). Since the effect of both fiber density and myelination on FA cannot be separated straightforwardly, we shall refer to them jointly as White Matter Architecture of the single bundle of fibers (WMAS).

In this work, we explore the possible neuroanatomical determinants of P_α through individual subjects taken from the database of the Cuban Human Brain Mapping Project (CHBMP). The CHBMP is suitable for this purpose since it combines structural Magnetic Resonance Imaging (MRI), Diffusion-Weighted Magnetic Resonance Imaging (DT-MRI) and EEG information (Udulag et al., 2008). We reexamine the results reported in Nunez et al. (1978), but this time by automatically assessing head size with improved precision for 222 individuals, based on their T1-weighted MRIs. Furthermore, we calculate NSA and we assess the relation between its logarithm and that of the P_α, as claimed by the EEG cortical standing wave theory (Nunez et al., 1995).

Additionally, we explore, for the first time, an empirical relationship between WMAS and the P_α based on a multivariate penalized regression (Vega-Hernandez et al., 2008). We present and discuss which tracts, as defined by Regions-Of-Interest in Mori et al. (2008) and Hua et al. (2008), might be related with the P_α.

The phenomenological findings of this paper inspire future work exploring biophysical explanations by means of mathematical modeling of the generation of the alpha rhythm.

Materials and methods

Notation

A lower case bold symbol, e.g. $\mathbf{h}_{n\times 1}$, denotes a *column vector* of length n. An upper case symbol, e.g. $\mathbf{A}_{n\times m}$, denotes a *matrix*, whose size is specified by the corresponding subscripts. Nonbold symbols denote *scalar magnitudes*. The superscript T denotes *transpose*. $||\mathbf{a}||$ is the *Frobenius norm* of $\mathbf{a}$. $\mathbf{1}_n$ is a column vector of n ones, $\mathbf{1}_{n\times m}=\mathbf{1}_n\mathbf{1}_m^T$ is an $n\times m$ matrix of ones, $\mathbf{I}_n\times_m$ is the identity matrix and $\mathbf{H}=\mathbf{I}_{m\times m}-(\mathbf{1}/m)1_{m\times m}$ is the *centering* operator. The symbol $\wedge$ is the logical operator AND, while the natural logarithm of x will be denoted by $\log(x)$.

Acquisition and preprocessing of MRI data

As part of the Cuban Human Brain Mapping Project, using a Siemens Symphony 1.5 T, we sampled MRI data of 397 healthy subjects from the Cuban population. They were initially a subset of a larger sample (1574) randomly targeted from the Cuban National ID registry that was submitted to neuropsychiatric and neuropsychological tests. Those who were considered by an expert panel as healthy provided, after written consent, our current MRI data set which consists of 3D MPRAGE structural T1-weighted images with $1\times1\times1$ mm^3 voxel size and dimensions of $160\times256\times256$. We used TR/TE/TI = 3000/3.93/1100 ms. After visual quality control by an expert, the final number of selected T1-weighted images was $N_{T_1}=305$.

We also acquired, using a single-shot EPI, six repetitions of diffusion-weighted images (DWIs) for 12 directions of the diffusion gradient with $b=1200$ s/mm^2 and a nondiffusion-weighted image (B0:$b=0$ s/mm^2). The number of slices was adapted to cover the whole brain, with a thickness of 3 mm, in-plane resolution of 2×2 mm^2 and FOV of 128×128 mm^2. TE was 160 ms. Magnitude and phase images were also acquired using a gradient echo sequence with $TE_1=7.71$ ms and $TE_2=12.47$ ms. All DWIs were visually inspected and those which presented either technical or pathological defects were discarded. This quality control process led to a final sample of DWIs of 172.

Head size and cortical surface areas

We calculated four measures of head size for every subject in a fully automated procedure. For this, we first normalized, using SPM nonlinear registration (cutoff = 25 mm) the T1 image to the MNI-152 average brain (Mazziotta et al., 2001). The linear part of this transformation was used to map the plane $z=0$ in the MNI space to the individual one. We extracted the curve defined by the intersection between the scalp surface and the transformed plane. The scalp was extracted using FSL (Smith, 2002). The length of this curve was calculated as the first measure of head size. We also marked nasion, inion and both preauricular points in the MNI-152 average brain using IMAGIC software (Neuronic S.A www.neuronicsa.com). With the whole transformation, these points were mapped to the individual space and projected to the scalp surface. The distance between individual nasion and inion and between the individual preauriculars was calculated as the second and third measure of head size, respectively. The fourth measure was the geometrical mean of the first three measures, i.e. the cubic root of their product, as proposed in Nunez et al. (1978).

The surface of the neocortex for each subject was extracted using CLASP (http://wiki.bic.mni.mcgill.ca/index.php/CLASP) (Kim et al., 2005), software kindly provided by the Montreal Neurological Institute. Each cortical surface is the mean surface between the white/gray matter interface and the gray matter/cerebrospinal fluid interface with a tessellation of 81,920 faces and approximately 41,000 vertices. The patches joining the hemispheres in the medial plane (initially included for obtaining closed surfaces) were removed to calculate the total surface area as the sum of the areas of the faces.

DTI fractional anisotropy

A mild Gibbs ringing artifact around the ventricles in the B0 images was corrected with a Hanning filter. Eddy current and motion effects were also corrected by linear registration of the weighted images to the B0. With the aid of phase and magnitude images, we corrected distortion effects due to main field inhomogeneities using the Unwarping SPM2 toolbox (Anderson et al., 2001).

Diffusion tensors were fitted for every voxel using a robust linear regression method (Le Bihan and van Zijl, 2002). We computed the FA images for all the subjects and, in order to achieve anatomical correspondence among them, performed the following procedure:

1. A random FA image of the sample was normalized to the FA template provided online by the ICBM (ICBM-DTI-81 (Mori et al., 2008) using SPM5 with a the Discrete Cosine Transform expansion cutoff of 25 mm (Ashburner and Friston, 1999). This was the first reference image of an iterative procedure described in the next steps.

Please cite this article as: Valdés-Hernández, P.A., et al., White matter architecture rather than cortical surface area correlates with the EEG alpha rhythm, NeuroImage (2009), doi:10.1016/j.neuroimage.2009.10.030

2. Using a high dimensional nonlinear registration method (Thirion, 1998) based on FA intensities, all individual FA images were normalized to the reference FA image and averaged in order to build a new reference image.
3. Step 2 was repeated three times using, at each time, the updated average FA image as reference.

Three further subjects were discarded after a visual quality control of the registered images, keeping a total of $N_{DWI} = 169$ subjects.

As mentioned in the Introduction, FA is used to characterize WMAS in single bundle profile voxels. However, the WMAS-FA dependence is no longer valid for multiple bundle profiles, such as crossing, bending, kissing or merging of more than one bundle in a voxel. Since multiple bundle profile voxels are characterized by very low values of FA, we shall only quantify WMAS in those voxels where the FA is above 0.2 (Salat et al., 2005). This condition does not eliminate all the voxels with multiple profiles, but at least, reduces the cases where the angle between coexisting bundles is large, which is precisely where FA is more independent from WMAS.

For every i-th FA image, we created a binary mask, M_i, imposing a TRUE value for the voxels satisfying the threshold condition. A final mask M, more restrictive, was calculated as:

$$M = M_1 \wedge M_2 \wedge \cdots \wedge M_{N_{DWI}} \wedge WM, \tag{1}$$

where WM is a mask of white matter. WM is calculated as follows:

$$WM = (P_{WM} > P_{GM}) \wedge (P_{WM} > P_{CSF}) \wedge (P_{WM} > 1 - P_{GM} - P_{WM} - P_{CSF}), \tag{2}$$

with P_{GM}, P_{WM} and P_{CSF} being the probabilistic images of gray matter, white matter and cerebrospinal fluid, respectively, provided by SPM5. The values of every warped individual FA image, corresponding to the N_v TRUE voxels of M, were arranged into row vectors.

Acquisition and preprocessing of electroencephalography

Ten minutes *eyes closed* (condition suitable for measuring global alpha rhythm) electroencephalographic recordings were carried out using a MEDICID-05 (www.neuronicsa.com) from two scalp electrodes, each located at the most occipital sites (O1 and O2) of each hemisphere, precisely where the alpha activity is usually strongest (Niedermeyer and Lopes da Silva, 2004). The signals were digitized with a sampling frequency of 200 Hz. A band pass finite impulse response filter (order = 128) with a Kaiser window ($\beta = 0.5$) was applied to the channels (Oppenheim and Schafer, 1989), with cutoff frequencies of 0.1 and 45 Hz. Filtering was performed in forward and reverse mode to guaranty zero-phase distortion (Gustafsson, 1996). The resulting time series, for each channel, were segmented into time intervals (epochs) of 2.56 s, i.e. 512 points, which were assumed to represent a large number of realizations of the same electrophysiological process. An expert electroencephalographer eliminated, based on visual inspection, the epochs presenting artifacts (due to drowsiness, ocular movements or extreme noise). The remaining epochs were multiplied with a Hamming window to improve the spectral estimates obtained by the Fast Fourier Transform in a frequency interval of 0.39 to 29.69 Hz, with a resolution of 0.39 Hz ($N_w = 76$ frequency values). The average spectrum across epochs of each electrode was computed for each subject. After the quality control described above, the number of subjects having EEG was $N_{EEG} = 232$. As in Posthuma et al. (2001), we calculated the maximum value within 7 to 14 Hz of the power spectrum of each electrode. Given the very high correlation found between the spectra of both electrodes, the alpha frequency (P_α) was taken as the average of the spectral positions of the maxima. The mean of the values of P_α in our sample is 9.9416, which is close to previously reported values (Aurlien et al., 2004), and the standard deviation is 0.8338.

Ages are within the range from 18 to 45 years. We assess correlations between both P_α and FA with age to discard the effect of this in our analyses and results.

Final data sets

We organized the data sets obtained above by constructing the following mathematical structures:

1. A vector $\mathbf{h}^{ax-perim}_{N_{T_1} \times 1}$ containing the first measure of head size, namely the axial perimeter, for the N_{T_1} subjects.
2. A vector $\mathbf{h}^{ant-post}_{N_{T_1} \times 1}$ containing the second measure of head size, namely the anterior–posterior distance, for the N_{T_1} subjects.
3. A vector $\mathbf{h}^{preauric}_{N_{T_1} \times 1}$ containing the third measure of head size, namely the distance between the preauricular points, for the N_{T_1} subjects.
4. A vector $\mathbf{h}^{cubic}_{N_{T_1} \times 1}$ containing the fourth measure of head size proposed by (Nunez et al., 1978), namely cubic root of the product of the first, second and third head measures, for the N_{T_1} subjects.
5. A vector $\mathbf{S}_{N_{T_1} \times 1}$ containing the neocortical surface area for the N_{T_1} subjects.
6. A vector $\alpha_{N_{EEG}} \times 1$ containing the P_α for the N_{EEG} subjects.
7. A 2D matrix $A_{N_{DWI} \times N_v}$ with the N_{DWI} FA images, ordered in row vectors of N_v elements corresponding to voxels.

Relation between head size measures and the alpha frequency

In the theory presented in Nunez et al. (1995), electrical activity propagates from one cortical region to the next (either along collaterals or white matter axons) like traveling waves over the neocortical surface, which is topologically spherical. This is a finite medium so traveling waves can interfere to form standing waves. In an exploratory analysis assuming very simple properties of the wave medium, i.e. assuming undamped, nondispersive and free oscillations, the eigenmodes are the Spherical Harmonics functions Y_{lm}, $l = 1,2,3,\ldots$; $m = -l, -(l-1), \ldots, 0, \ldots, (l-1), l$, $l = 1,2,3\ldots$, $m = -l, -(l-1), \ldots, 0, \ldots, (l-1), l$, and the eigenfrequencies, ω_l (corresponding to the index l), result to be inversely proportional to the radius, R, of the neocortical equivalent sphere:

$$\omega_l \propto \sqrt{l(l+1)}\frac{v}{R}, \quad l = 1, 2, 3, \ldots \tag{3}$$

where v is the wave conduction velocity. In this theory, the alpha frequency is assumed to correspond to the first eigenmode ($\alpha F \equiv \omega_{l=1}$) since $\omega_{l=1}$ is around the typical value of 10 Hz. The proportionality trend between spatial and temporal frequencies still holds for slightly damped waves so a relation like Eq. (3) can be still used to describe the actual brain dynamics in the cortical standing wave theory of the EEG.

Since the area of the equivalent sphere is that of the neocortex surface (NSA), the square root of the latter can substitute for R in the relation above. However, at the time of the original study (Nunez et al., 1978), it was not possible to measure NSA *in vivo* with acceptable precision. Therefore, they proposed to use the fourth head size measure defined in this paper as a proxy for NSA, assuming a fixed ratio of the NSA to the external head area (the *cortical folding factor*). The significant negative correlation obtained in Nunez et al. (1978) supported Eq. (3). However, the folding factor can vary from subject to subject (Mangin et al., 2004). Fortunately, we are able to measure NSA directly from MRI. We therefore substitute its square root for R in Eq. (3) and apply the natural logarithm to both members, obtaining:

$$\log(\alpha F) = -1/2\log(\mathrm{NSA}) + C, \tag{4}$$

where C is an undetermined constant.

We first investigate the validity of the relation obtained in Nunez et al. (1978) by assessing the Pearson correlation between $\alpha_{N_{T_1-EEG} \times 1}$ and $h^{cubic}_{N_{T_1-EEG} \times 1}$, where $N_{T_1-EEG} = 222$ is the number of subjects having

Please cite this article as: Valdés-Hernández, P.A., et al., White matter architecture rather than cortical surface area correlates with the EEG alpha rhythm, NeuroImage (2009), doi:10.1016/j.neuroimage.2009.10.030

both T1-weighted and EEG simultaneously. We also determine which, among the four head size measures defined in this paper, has the highest correlation with NSA, being the actual best representative of the latter. Additionally, the value of this correlation quantifies the variability of the folding factor and therefore the validity of Nunez's assumption. We then calculate the Pearson correlation between the NSA-representative head measure and $\alpha_{N_{T_{1-EEG}}\times 1}$. Finally, to validate Eq. (4), we carried out a linear univariate robust regression (DuMouchel and O'Brien, 1989) between vectors $\log\left(\alpha_{N_{T_{1-EEG}}\times 1}\right)$ and $\log\left(s_{N_{T_{1-EEG}}\times 1}\right)$. This would allow comparing the estimated slope with the theoretical value of $-1/2$.

RIDGE regression between fractional anisotropy and the alpha frequency

In order to study the relationship between P_α and FA, we propose the following linear model:

$$\alpha_{m\times 1} = A_{m\times N_v}\beta_{N_v\times 1} + 1_m\beta_0 + \varepsilon_{m\times 1}, \tag{5}$$

where $m = N_{EEG\text{-}DTI} = 89$ is the number of subjects having both EEG and DTI simultaneously, and the vector $\boldsymbol{\varepsilon}$ represents a multivariate Gaussian error.

We conveniently define $\hat{\mathbf{A}} = \mathbf{HA}$ and $\hat{\boldsymbol{\alpha}} = \mathbf{H}\boldsymbol{\alpha}$. Both are measures of the deviation of each individual from the average across subjects. Given that $\mathbf{H}\,(1_m\,\beta_0) = 0$ and $\mathbf{H}\boldsymbol{\varepsilon} = \boldsymbol{\varepsilon}$, Eq. (5) can be easily transformed into:

$$\hat{\alpha} = \hat{A}\beta + \varepsilon \tag{6}$$

Using a sparse discrete $N_v \times N_v$ Laplacian $\mathbf{L}$, as the penalizing operator, the solution of the so-called RIDGE regression (Vega-Hernandez et al., 2008) is given by $\hat{\beta} = \underset{\beta}{arg\,min}\,||\,\hat{\alpha} - \hat{A}\beta|\,^2 + \lambda||\,L\beta||\,^2$, with λ being the regularization parameter. The analytical form of this solution is:

$$\hat{\beta} = \left[X^T X + \lambda I_{N_v\times N_v}\right]^{-1} X^T\hat{\alpha}, \tag{7}$$

where $\mathbf{X} = \hat{\mathbf{A}}\mathbf{L}^{-1}$. An optimal value for λ is obtained by minimizing the generalized cross validation function (Vega-Hernandez et al., 2008). The intercept is estimated as $\hat{\beta}_0 = 1/m\ \mathbf{1}_m^T\ (\boldsymbol{\alpha} - \mathbf{A}\hat{\boldsymbol{\beta}})$. The use of a quadratic penalty based on the Laplacian of the coefficient copes with the ill-posed condition of the problem in the sense of Hadamard. This constraint imposes smoothness between the coefficients, which is justified if we assume that the development and architecture of tissue between neighboring voxels are a correlated process.

Statistical significance

The bootstrapping methodology suggested in Paparoditis and Politis (2005) was used for assessing the coefficients $\hat{\boldsymbol{\beta}}$, obtained with Eq. (7), that are significantly different from zero. Using Eq. (6), a vector of residuals $\hat{\varepsilon} = \hat{\alpha} - \hat{A}\hat{\beta}$ is estimated. Under the null hypothesis of no linear relation, i.e. H_0: $\boldsymbol{\beta} = \mathbf{0}$, pseudo-observations are generated by adding a noise vector to the intercept, i.e. $\hat{\alpha}_j^* = \varepsilon_j^*$, where the components of ε_j^* are drawn from the empirical distribution of the estimated residuals (vector $\hat{\varepsilon}$). This is done for $j = 1,\ldots, 10^5$ bootstraps. The estimators of $\hat{\boldsymbol{\beta}}$, under the null hypothesis, say $\hat{\beta}^*_{H_0}$, are also calculated for all bootstraps. Being $S_{\theta^*_{H_0}}$ the variance of $\hat{\beta}^*_{H_0}$, we constructed the "studentized" pivotal statistics, $\hat{t}^*_{H_0} = \sqrt{N_{EEG-DWI}}\,\hat{\beta}^*_{H_0}/\sqrt{S_{\theta^*_{H_0}}}$ and $\hat{t} = \sqrt{N_{EEG-DWI}}\,\hat{\beta}/\sqrt{S_{\theta^*_{H_0}}}$, which are suitable to maximize the power of the test (Paparoditis and Politis, 2005). To avoid the inflation of type I error, due to the experiment-wise error for the simultaneous univariate comparisons, a negative and a positive global multivariate threshold, based on all $\hat{t}^*_{H_0}$, have to be established in order to find those negative and positive components of $\hat{\mathbf{t}}$ respectively for which it is possible to reject the null hypothesis with certain probability. Thus, we define the "0.5; 99.5" statistics, which are slightly less conservative, but reliable, versions of the min-max statistics proposed in Galán et al. (1994). These are calculated for each bootstrap as the 0.5 and 99.5 percentile of the values of $\hat{t}^*_{H_0}$. Having the distributions of both statistics, the negative threshold, t_-, is chosen as the α percentile of the "0.5" statistic whereas the positive, t_+, is set at the $100 - \alpha$ percentile of the "99.5" one. This allows for the determination of the significant negative and positive (nonzero) components of $\hat{\mathbf{t}}$, and therefore of $\hat{\boldsymbol{\beta}}$. With $\alpha = 1$, we set to zero the nonsignificant components to obtain a new vector, $\hat{\boldsymbol{\beta}}_{0.5/1}$ (using the notation $\hat{\boldsymbol{\beta}}_{s/\alpha}$ to refer to the "s;$100 - s$" statistic, whereas α refers to the percentile calculated from the "s;$100 - s$" statistic). Let $p\ t = Tcdf\ t$ be the cumulative distribution function of the histogram of all elements of $\hat{\mathbf{t}}$. This is the probability of a certain test, t, to satisfy H_0: $t = 0$. The statistical significance of both the negative and positive values of $\hat{\beta}_{0.5/1}$ is therefore $p_- = Tcdf\ t_-$ $p_+ = 1 - Tcdf\ t_+$.

The values of the elements of $\hat{\beta}_{0.5/1}$ can be arranged into the FA template image with the corresponding values for each voxel. In the resulting image, we can find clusters of significant coefficients. To reduce possible spurious results, we also set to zero the values of the coefficients of $\hat{\beta}_{0.5/1}$ corresponding to those clusters with a volume below 150 mm^3, as in Stufflebeam et al. (2008). Aided by the ICBM-DTI-81 Atlas (Mori et al., 2008) and that presented in Hua et al. (2008), which we shall name simply Fiber Atlas (see Table 1), we also identify the major bundle of tracts containing significant clusters of $\hat{\beta}_{0.5/1}$.

To assess whether the results of this paper hold with even more conservative criteria, we obtained also the $\hat{\beta}_{0/1}$ estimator, by using the min–max (i.e. "0 – 100") statistics, which is proposed in Galán et al. (1994), and $\alpha = 1$. This time, the clusters below 100 mm^3 were removed.

The regression method described above is also used in this work to assess the relation between both age and head size with FA.

RIDGE regression between head size and FA

Our sample has a considerable variation across head sizes. According to the theoretical considerations in Appendix B, FA should not depend on the head size. However, this has to be proven experimentally. If head size constitutes a source of FA variance, it has to be taken into account to decrease the percentage of unexplained variance in the P_α-FA regression model.

We investigated the possible relation between FA and the different size measures defined in this paper as well as the radius of the equivalent neocortical sphere $\sqrt{\mathbf{s}}$. For this, we substituted $\boldsymbol{\alpha}$ for the desired measure in the RIDGE regression model described in this subsection. We also used the logarithms of the size measures to account for different possible forms of the FA-size relationship.

Results and discussion

No significant correlation was found between age and P_α in our sample ($p > 0.05$). This is in agreement with Aurlien et al. (2004). Moreover, the coefficients of the regression between age and FA became statistically nonsignificant ($p > 0.05$) beyond a few iterations of the bootstrapping procedure. In fact, for the range of ages of our sample, very slight correlation has been found between age and FA in some voxels (Moseley, 2002b; Salat et al., 2005; Sullivan and Pfefferbaum, 2006). We will discard the effect of age on our data sets for the posterior analyses.

Relation between the alpha frequency and the head size measures

Fig. 1 shows a plot of the neocortical surface area (NSA) versus each head size measure and their corresponding correlations. The highest correlation is with the anterior–posterior distance (the first measure, i.e. the nasion to inion distance). Thus, this is the best

Please cite this article as: Valdés-Hernández, P.A., et al., White matter architecture rather than cortical surface area correlates with the EEG alpha rhythm, NeuroImage (2009), doi:10.1016/j.neuroimage.2009.10.030

Table 1
Possible tracts and ROIs containing significant nonzero clusters of the multivariate regression estimators.

Fiber bundles (*longitudinal fascicles, projection or association fibers*)	Statistical significance	Sign of the relation	ROIs with significant clusters according to the ICBM-DTI-81 (Mori et al., 2008) Atlas and the Fiber Atlas (Hua et al., 2008)
Thalamocortical or corticothalamic fibers			
Posterior Corona Radiata and Superior Corona Radiata in both the right and left hemispheres	$p<0.00044$	Positive	ICBM-DTI-81 Atlas: Posterior Corona Radiata Left (PCR-L), Superior Corona Radiata Left (SCR-L), Posterior Corona Radiata Right (PCR-R), Superior Corona Radiata Right (SCR-R). We suggest that this significance is associated to thalamocortical (TC) interactions since there is no significance in the Body of the Corpus of Callosum or corticofugal pathways, both also passing trough CR.
Posterior Thalamic Radiation in the right hemisphere	$p<0.00045$	Negative	ICBM-DTI-81 Atlas: Posterior Corona Radiata Right (PCR-R).
Anterior Thalamic Radiation in the right hemisphere	$p<0.00045$	Negative	ICBM-DTI-81 Atlas: Anterior Corona Radiata Right (ACR-R).
Commissural fibers			
Inferior Splenium and Major Forceps[a]	$p<0.0000025$[a]	Negative	ICBM-DTI-81 Atlas: Splenium of the Corpus Callosum (SCC). Fiber Atlas: This suggests that the significance is predominantly within the Major Forceps, i.e. fibers connecting the inferior Occipital Lobes.
Isthmus and Tapetum[a]	$p<0.0000028$[a]	Positive	ICBM-DTI-81 Atlas: Superior part of the SCC, Tapetum Right (TAP-R) and Tapetum Left (TAP-R). This suggests a positive significance within the commissural fibers connecting the superior Occipital Lobes.
Association fibers			
Inferior Fronto-Occipital Fascicle (IFO) in the left hemisphere	$p<0.00044$	Positive	ICBM-DTI-81 Atlas: Sagittal Stratum Left (SS-L), the External Capsule Left (EC-L) and the Inferior Fronto-Occipital Fasciculus Left (IFO-L), all of them containing the IFO. Fiber Atlas: This suggests that the significance is predominantly within the IFO and ILF bundles.
Inferior Longitudinal Fascicle (ILF) in the left hemisphere	$p<0.00044$	Positive	ICBM-DTI-81 Atlas: SS-L, which contains the ILF. Fiber Atlas: This suggests that the significance is predominantly within the IFO and ILF bundles.
Inferior Fronto-Occipital Fascicle (IFO) in the right hemisphere	$p<0.00045$	Negative	ICBM-DTI-81 Atlas: Sagittal Stratum Right (SS-R), the External Capsule Right (EC-R) and the Inferior Fronto-Occipital Fasciculus Right (IFO-R), all of them containing the IFO. Fiber Atlas: This suggests that the significance is predominantly within the IFO and ILF bundles.
Inferior Longitudinal Fascicle (ILF) in the right hemisphere	$p<0.00045$	Negative	ICBM-DTI-81 Atlas: SS-R, which contains the ILF. Fiber Atlas: This suggests that the significance is predominantly within the IFO and ILF bundles.

[a] Tracts with the highest significance.

representative of NSA, instead of the fourth head size measure, which was used in Nunez et al. (1978), namely the cubic root of the product of the anterior–posterior distance, the preauricular distance and the cephalic perimeter. All correlations were highly significant so the use of a head size measure as an approximate of NSA was appropriate in Nunez et al. (1978).

Fig. 2a shows a plot of the alpha frequency (P_α) versus the nasion to inion distance. Contrary to Nunez et al. (1978), although still negative, the Pearson correlation ($r=-0.04$) is not significantly different from zero ($p=0.55$). Fig. 2b shows the log(P_α) versus log (NSA) plot. The slope of their regression is −0.0558 with a confidence interval of −0.123 0.005 which not only includes zero but also excludes the theoretical value predicted by Eq. (3), which is −1/2.

Although the Eq. (3) was derived from simple linear approximations of the wave equation, for which the eigenmodes are the Spherical Harmonics (Nunez et al., 1995), the NSA-P_α inverse relation would still be valid even for more complicated versions of the theory of cortical standing waves, taking into account the actual properties of the medium and geometry of the head (Nunez et al., 1995; Nunez and Srinivasan, 2006), which is highly nonlinear, inhomogeneous, dispersive and with complicated connectivity patterns. Thus, the prediction of the EEG cortical standing wave theory, at least in its present formulation, is not supported by our results.

There are additional conceptual difficulties with the existence of a significant NSA-P_α relation, even for the case when Eq. (3) holds. As recognized by Nunez et al. (1995), the assumption of a constant value of the axonal conduction velocity (CV) for all head sizes may not be valid. Head size might conceivably be directly proportional to CV if conduction times are biological constants. In this case, $v/R=cons$ in Eq. (3) predicts a constant P_α irrespective of head size. Proportionality between CV and head size is in fact supported by evidence in the literature: (1) the well known linear relation between CV and myelin sheath thickness (Goldman and Albus, 1968; Rushton, 1951; Sabah, 2000; Waxman, 1980), 2) the possible positive relation between myelin sheath thickness and fiber length (Chen et al., 1992; Hursh, 1939a), and finally (3) the reasonable direct proportionality between fiber length and head size, since larger heads imply connected regions to be one further from each other. Indeed, Hursh (1939b) experimentally proved that CV increases with developing cat's head size increases, while Eyre et al. (1991) found a constancy of time delays for human development. Furthermore, Salami et al. (2003) suggested, based on striking experimental results in mice, that thalamocortical fiber length modulates myelination, and thus conduction velocity, to keep latency constant irrespective of how distant the connected structures are. The intra- and inter-species positive relation between CV and brain size, by modulation of axon thickness, is experimentally presented and discussed in Wang (2008) as a consequence of conduction optimization.

The relation between the alpha frequency and the fractional anisotropy image

We firstly performed the regression between head size and FA. The coefficients became statistically nonsignificant beyond the 1000 iteration of the bootstrapping procedure. This gives experimental evidence for the theoretical considerations in Appendix B: FA changes are due microstructural variations not related to head size. Based on this and the obtained results in the subsection above, we can discard a possible effect of head size on both FA and P_α.

We then performed the regression analysis between the centered fractional anisotropy matrix $\hat{\mathbf{A}}$ and the centered alpha frequency vector $\hat{\boldsymbol{\alpha}}$ (Eq. (6)). The significant nonzero estimates of the coefficients of the solution of this equation, under the smoothness condition (Eq. (7)), i.e. both $\hat{\beta}_{0.5/1}$ and $\hat{\beta}_{0/1}$, are overlaid on the template FA image (Fig. 3). These vectors correspond to the "0.5;99.5" and "'0;100" pairs of statistics, respectively, with $\alpha=1$. The interpretation of this image

Please cite this article as: Valdés-Hernández, P.A., et al., White matter architecture rather than cortical surface area correlates with the EEG alpha rhythm, NeuroImage (2009), doi:10.1016/j.neuroimage.2009.10.030

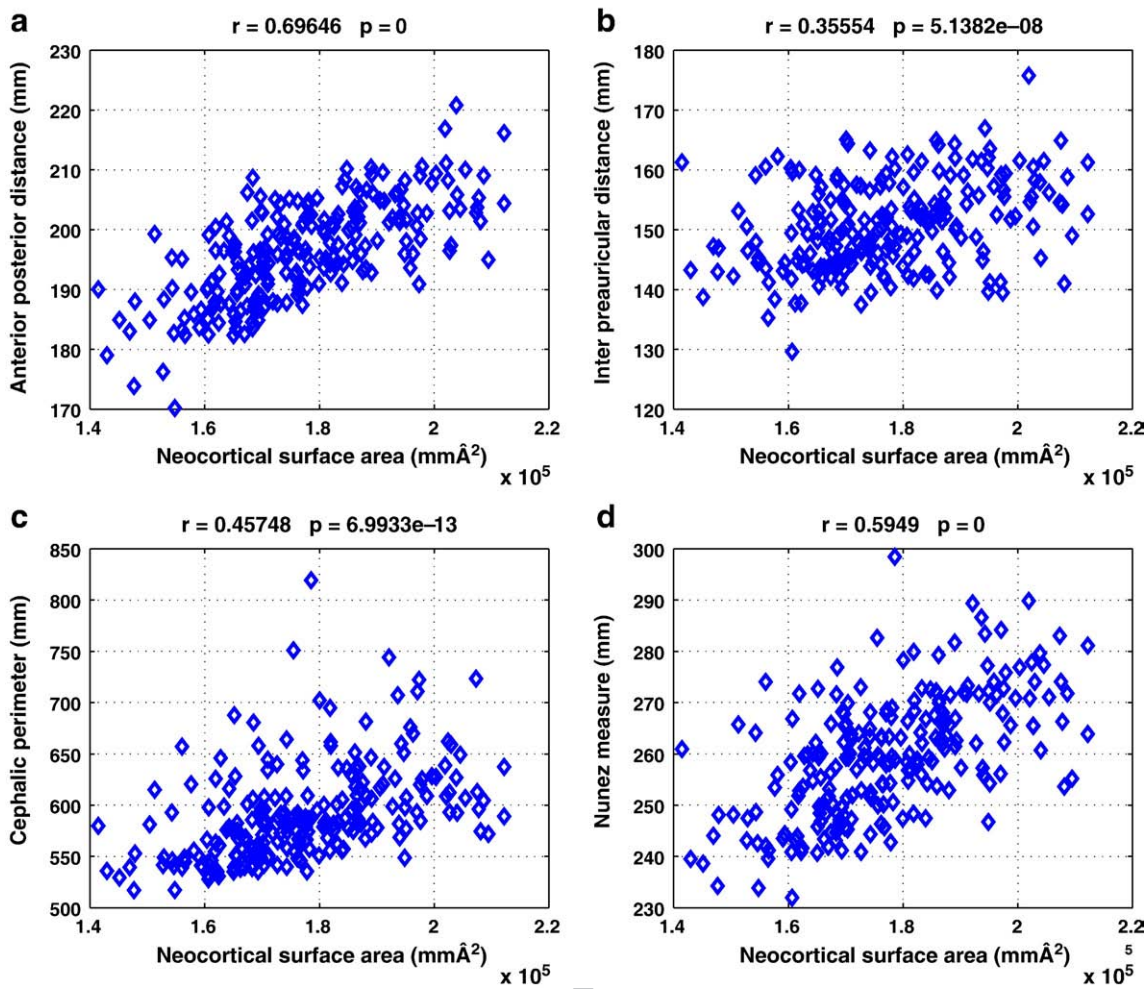

Fig. 1. Scatter plot of (a) anterior–posterior distance (AP) vs. neocortical surface area (NSA), (b) inter-preauricular distance vs. NSA, (c) cephalic perimeter vs. NSA, (d) Nunez's head measure $\left(\sqrt[3]{AP \times LR \times CP}\right)$ vs. NSA. The correlation and *p*-values are shown above each scatter plot.

is straightforward. For voxels corresponding to negative (positive) components of $\hat{\beta}_{0.5/1}$, FA is inversely (directly) proportional to P_α. Besides, the intercept is $\hat{\beta}_0 = 10.05$ *Hz*, and represents the predicted P_α for the average FA, being closer to its mean value. Note that this corresponds to the commonly accepted typical value of P_α in a normal subject (≈ 10 *Hz*).

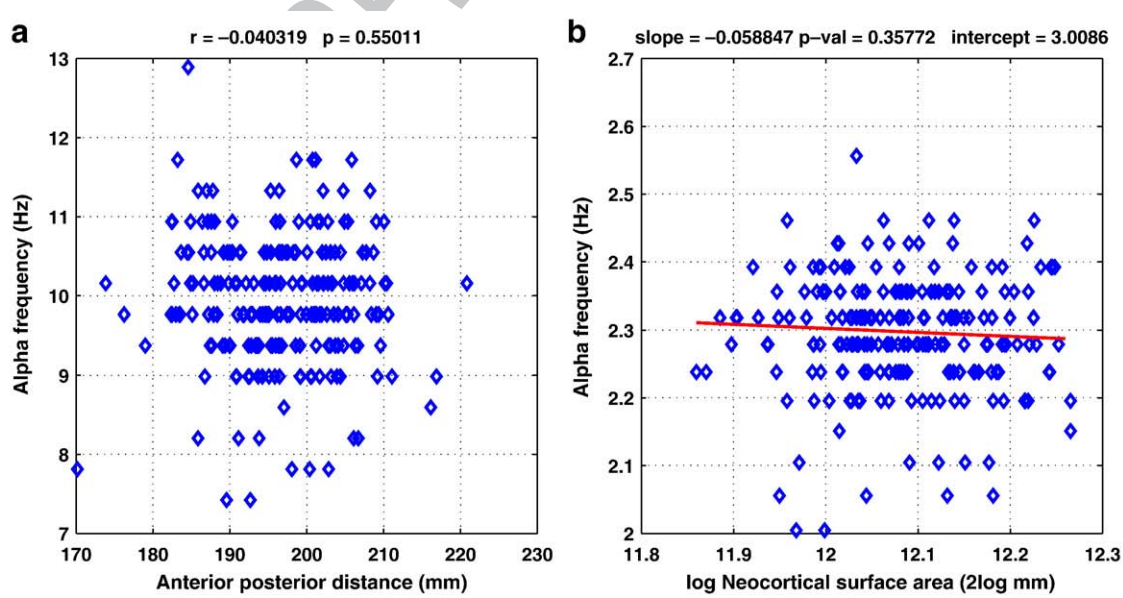

Fig. 2. Scatter plot of (a) P_α vs. AP with their correlation and *p*-value and (b) log(NSA) vs. P_α with their regression slope and *p*-value.

Please cite this article as: Valdés-Hernández, P.A., et al., White matter architecture rather than cortical surface area correlates with the EEG alpha rhythm, NeuroImage (2009), doi:10.1016/j.neuroimage.2009.10.030

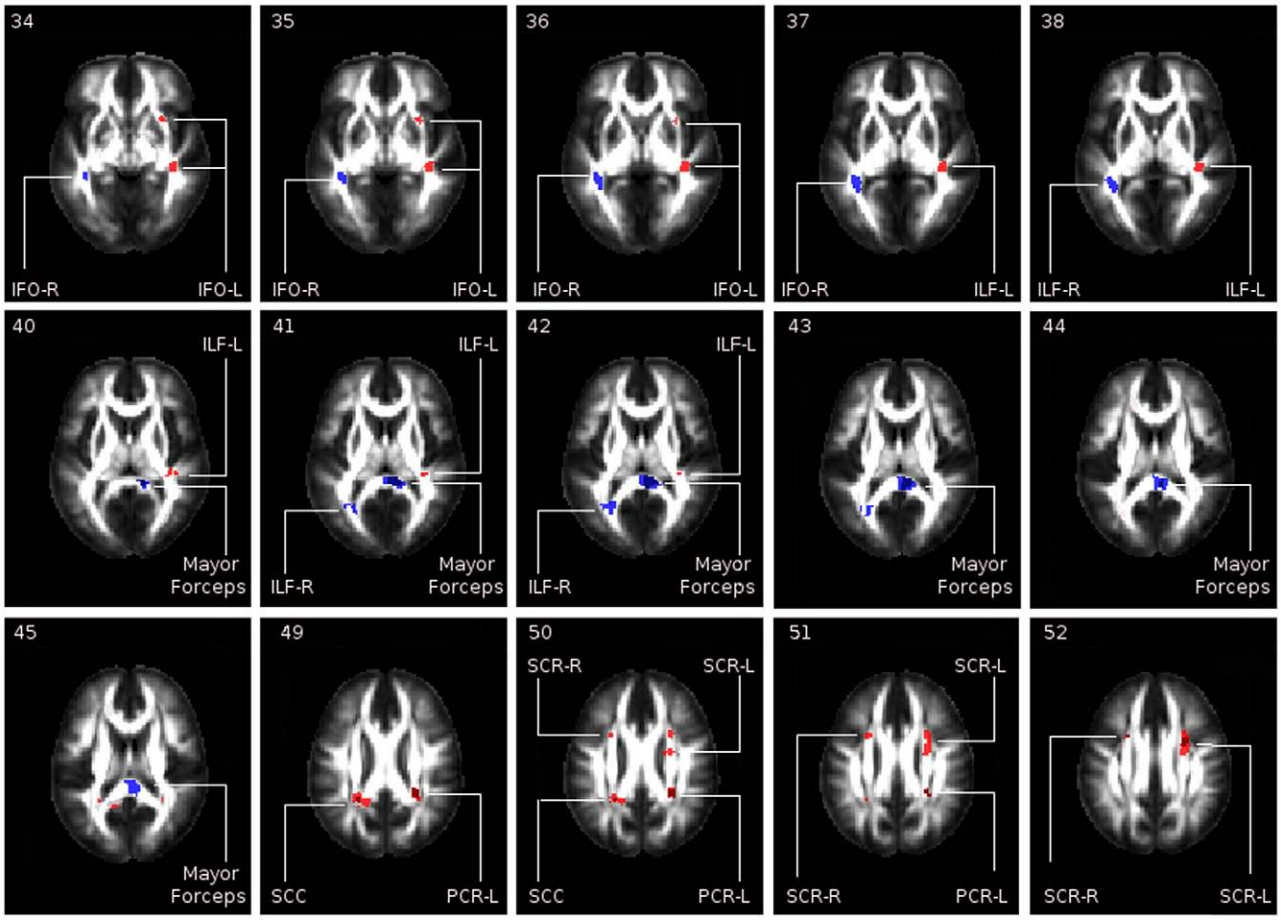

Fig. 3. Significant nonzero estimates of the coefficients of $\hat{\beta}_0^{"0.5/1"}$. The values are overlaid on the template FA image. The names of the significant clusters of $\hat{\beta}_0^{"0/1"}$ are outlined. IFO, Inferior Fronto-Occipital Fasciculus; ILF, Inferior Longitudinal Fasciculus; SCC, Splenium of the Corpus Callosum; PCR, Posterior Corona Radiata; SCR, Superior Corona Radiata.

The uncorrected p-values are $p \leq 0.0004$ for the "0.5;99.5" statistics and $p \leq 0.0002$ for the "0;100" statistics (see also Table 1). A value of $\alpha = 1$ corresponds to $p \leq 0.01$ corrected for multiple comparisons. These p-values are smaller to those in Stufflebeam et al. (2008) ($p \leq 0.001$ uncorrected and $p \leq 0.05$ corrected for multiple comparisons). Moreover, we used 10^5 iterations in the bootstrap procedure, which is a higher value than that used in Stufflebeam et al. (2008), which was 10^4. We are considering that work as a reference, regarding the statistical procedure, since it is the only reporting a relation between FA and an electrophysiological variable.

The FA, in the voxels corresponding to the significant components of $\beta_{0.5/1}$, only explains the 25% of the P_α variance for the linear multivariate model. This is probably due to other sources of variance that are not taken into account in the model. For example, according to Appendix A and B, a change in fiber length irrespective of head size leads to an inversely proportional change in time delays and therefore P_α, without changing FA. Additionally other parameters, associated to the role of grey matter local dynamics, such as dendritic rise and decay times, nonlinearity thresholds, synaptic strength and density, number of neurons and short and long term plasticity, could be other sources of variance.

On the other hand, there are several neuroanatomical causes of variability of FA, which do not necessarily affect P_α. For example, according to the theoretical analysis in Appendix A and B, a change in bundle thickness irrespective of head size, keeping the number of fibers constant, leads to an inversely proportional change of fiber density and therefore FA, without change in connectivity and time delay and thus with no evident implications on the P_α.

We are currently exploring more detailed biophysical models relating white matter parameters, (such as those reflecting the importance of the connectivity pattern (Izhikevich and Edelman, 2008; Jirsa, 2009; Sotero et al., 2007; Valdes-Sosa et al., in press)) and neural mass model parameters (gray matter) to observable electrophysiological phenomena, as well as implementing very large-scale network simulations (Valdes-Sosa et al., in press) to test these and other issues.

White matter tracts with significant voxels

The ROIs containing voxels corresponding to significant nonzero coefficients of the RIDGE P_α-FA regression are summarized and commented in Table 1. They have been divided into three main groups corresponding to: longitudinal ipsilateral association fibers, thalamo-cortical projection fibers (or either corticothalamic feedbacks) and commissural fibers. An intriguing hemispheric asymmetry appears in the ipsilateral longitudinal tracts, with positive FA-P_α relation in the left and negative in the right. A positive FA-P_α relation is found in the Posterior and Superior Corona Radiata, probably associated to interactions between thalamus and cortex. Another intriguing result is the presence of significantly negative coefficients in the Posterior and Anterior Radiations only in the right hemisphere. The posterior commissural fibers of the Corpus Callosum present the most significant clusters of FA-P_α relationship, being negative in the inferior part (Splenium), connecting the inferior occipital lobes and positive in the superior part (Isthmus and Tapetum), connecting the superior occipital lobes.

Please cite this article as: Valdés-Hernández, P.A., et al., White matter architecture rather than cortical surface area correlates with the EEG alpha rhythm, NeuroImage (2009), doi:10.1016/j.neuroimage.2009.10.030

It is worth mentioning that the use of FA, as a neuroimage-based measure of WMAS, introduces two main disadvantages in the correct identification of ROIs where the WMAS might significantly determine P_α (1) the major presence of multiple fiber profiles, which could explain why significant clusters are not spread to parts of the tracts that are included in the mask; and (2) the masking condition, which could eliminate parts of or entire tracts. We believe, however, that masked FA is still an acceptable measure of WMAS, and is also easy to acquire with standard MRI protocols. Indeed FA-based white matter structural features have been successfully related to several variables in the literature, such as age (Camara et al., 2007; Moseley, 2002a; Pfefferbaum et al., 2000; Salat et al., 2005; Sullivan and Pfefferbaum, 2006), sex (Hsu et al., 2008; Szeszko et al., 2003), brain development (Ashtari et al., 2007; Courchesne et al., 2000; De Bellis et al., 2001; Giorgio et al., 2008; Schneiderman et al., 2007), behavioral variables (Deutsch et al., 2005) or reaction times (Madden et al., 2004; Stufflebeam et al., 2008). The work in Stufflebeam et al. (2008) demonstrates that FA correlates, in task-related anatomical regions, to electrophysiological events, as measured with MEG. As in this paper, these works usually apply a masking condition to the FA values.

Interpretation of the results

The significant relations between P_α and FA could be interpreted in the light of current theories of the genesis of the EEG, presented early in this paper, related to the possible effect of connectivity and time delay.

As mentioned before, FA is reflecting fiber density, myelination or a contribution of both. In particular, the results in Mädler et al. (2008), based on the voxel-wise regression between FA and Myelin Water Fraction (MWF), support the use of FA as a correlate of myelin in the Corona Radiata and Posterior White Matter (Splenium and Major Forceps). Therefore, our FA-P_α relation might be reflecting, in these ROIs, the effect of myelination on P_α, provided that the former determines the time delay of communication of the cortical areas connected by these tracts. It is believed that the alpha rhythms arise from highly synchronous cortical activity driven by the thalamus (Steriade et al., 1990). The positive feedback from cortex to thalamus forms a thalamo-cortico-thalamic closed loop. According to the simulations in Roberts and Robinson (2008) and Robinson et al. (2001c), P_α is most sensitive, and inversely proportional, to the period of this loop (twice the time delay between thalamus and cortex). Therefore, for the case of the Superior and Posterior Corona Radiata, the positive FA-P_α relation is expected provided that an increase in FA implies an increase of myelination. Note that these tracts mainly connect posterior cortices. This might be due to the following: (1) the highest alpha power is at occipital sites and/or 2) we are measuring the EEG at O1 and O2. To explain both cases, the posterior anatomical structures have to be the most influential. Although the closed eyes alpha is a global phenomenon arising from the cross-talk between different spatial scales (Nunez et al., 2001), the contribution of different localized structures are probably weighted by their proximity to the electrodes. In Robinson et al. (2003b), the contribution of posterior cortico-thalamocortical circuitry to the occipital scalp EEG is theoretically tackled by introducing spatially nonuniform corticothalamic and thalamocortical time delays.

The most significant clusters of P_α-FA relation are found in the occipito-occipital contralateral connections, precisely the circuitry connecting contralateral occipital cortices. This is coincidently the region where FA is more related with MWF in Mädler et al. (2008), giving further support to the possible role of myelin on P_α. However, the modulation of fiber density in connectivity cannot be discarded (Sotero et al., 2007). As can be seen in Table 1, there is evident sign variability in the P_α-FA relation among these contralateral connections. This might have several possible explanations. For example, we can consider that our measured P_α is the joint frequency of two neural masses in the "alpha regimen," each located at either posterior side of the brain. The simulations of David and Friston (2003) demonstrate that the correlation between the joint frequency and the time delay mediating their communication changes sign for different value ranges of the latter. Provided that there is a large variability of fiber lengths and myelination in the contralateral connections of the Corpus Callosum, time delays can fall in very different values ranges. On the other hand, the dual inhibitory and excitatory role described for the Corpus Callosum, involved in brain function integration and lateralization, respectively (Bloom and Hynd, 2008), might offer an alternative explanation for this sign variability. Also, it might be a possible negative influence of fiber density on conduction velocity due to an ephaptic interaction between fibers within a bundle, provoking an increase in time delay for higher couplings (Reutskiy et al., 2003). The Splenium of the Corpus Callosum might be particularly sensitive to this phenomenon since it presents a high fiber density (Barazany et al., 2009).

Although difficult to explain, the hemispheric asymmetry of the relation in the inferior longitudinal ipsilateral tracts and the Anterior and Posterior Thalamic Radiations might be due to the inter-hemispheric asymmetry of white matter (Buchel et al., 2004).

Conclusions

No correlation was found in a combined EEG/MRI data set (Cuban Human Brain Mapping Project) between head size and the spectral position of the alpha peak (P_α). This contrasts with the previous reports of Nunez et al. (1978) and Posthuma et al. (2001) where such a relation was found. Head size was considered by these authors to be proportional to the cortical surface area (NSA). However, the NSA is the actual variable that should best correlate with the EEG alpha rhythm according to a cortical standing wave theory of the EEG (Nunez et al., 1995), which predicts slightly damped traveling waves through the neocortex making the effect of boundaries on the dynamics of the alpha rhythm important. Our data allowed, for the first time, a direct validation of this theory by examining the relation between P_α and NSA due to the possibility for extracting the individual cortical surfaces. Even for this variable, there is no significant relation, as shown by the regression between the logarithms of both NSA and P_α. It therefore seems that, at least in its present form, the cortical standing wave theory of EEG generation is not supported by our data.

However, in our analysis of current biophysical models (e.g. Robinson et al., 2001b; Wright and Liley, 1996), the combination of global and local models predicts more damped alpha waves thus boundary conditions make little effect on P_α. Since large-scale interactions impinge the global character to the alpha rhythm, P_α should be more likely related to those white matter neuroanatomical determinants of connectivities and time delays. In fact, we found highly significant correlations between Diffusion Tensor Fractional Anisotropy (FA) and P_α, with no effect of head size on FA. This relation is significant for the ipsilateral longitudinal tracts, being positive in the left and negative in the right hemisphere. It is positive in the Posterior and Superior Corona Radiata, probably associated to interactions between thalamus and cortex. However, it is the posterior commissural fibers of the Corpus Callosum that present the most significant relations, being negative in the inferior part (Splenium), connecting the inferior occipital lobes and positive in the superior part (Isthmus and Tapetum), connecting the superior occipital lobes.

The results reported demonstrate that the use of large combined EEG/MRI databases allows empirical falsification of biophysical models of electrophysiological phenomena. Work in progress will provide more detailed biophysical models as well as large-scale network simulations, based on individual neuroanatomical measurements, in order to explore the nature of the relation between white matter architecture and the EEG spectrum in individual subjects.

Please cite this article as: Valdés-Hernández, P.A., et al., White matter architecture rather than cortical surface area correlates with the EEG alpha rhythm, NeuroImage (2009), doi:10.1016/j.neuroimage.2009.10.030

Studies of the neuroanatomical determinants of the EEG not only shed light on the basic mechanisms underlying electrophysiological processes, but also may serve to partial out spurious sources of variance for EEG spectral data allowing more insightful experimental findings and enhanced sensitivity in the evaluation of patients. Indeed, a reachable objective seems to be the integration of morphological and electrophysiological information in order to explain individual functional characteristics of a given subject.

Acknowledgments

We thank José Miguel Sánchez Bornot for his useful comments and programs for solving the multivariate regressions. Lídice Galán gave important advice in the statistical analyses of the data. We also thank Professor Alan Evans and his colleagues, from the Montreal Neurological Institute, for providing CIVET, the package of software used to extract all the cortical surfaces. The work presented in this paper was only possible thanks to the important contribution of all the members of the Cuban Human Brain Mapping Project, one of the National Programs of the Cuban Health Ministry.

Appendix A. A theoretical analysis of the effects of white matter microstructure on both the fractional anisotropy and the frequency of the alpha rhythm

Several studies have claimed that FA might be proportional to *fiber density* and *myelination* in the single bundle (Beaulieu, 2002; Hwang et al., 2003; Le Bihan, 2007). Indeed, according to simulations (Pabitra and Basser, 2005), FA is a monotonically increasing function, say $FA = \Phi\ f$, of the fraction of sectional area, $f \equiv ND^2/B^2$, occupied by N fibers of thickness D within a bundle of thickness B. Precisely $n \equiv N/B^2$ is the *fiber density*, and D reflects *myelination* (an increase of D is associated to an increase of the myelin sheath thickness if we assume a fixed value of axon diameter).

The connection of these microstructural parameters with the possible variables determining the alpha rhythm (*connectivity* and *time delay*) is straightforward. A rough estimate of connectivity is $C_0 = N$ whereas time delay is $t = L/v$, where L is the fiber length and v is the conduction velocity, which is proportional to D (Goldman and Albus, 1968; Rushton, 1951; Sabah, 2000; Waxman, 1980), i.e. $v = kD$, being k an arbitrary constant.

This suggests that FA might be directly related to connectivity and inversely related to time delay.

Appendix B. A theoretical analysis of the effects of head size on both the fractional anisotropy and the frequency of the alpha rhythm

Let us follow the notation in Appendix A and assume that the linear dimensions of any brain structure, e.g. the axonal fibers, are directly proportional to head size (Wang, 2008) (which we shall denote by R) and N is unchanged for different R (which is reasonable according to the inverse proportionality of fiber density and the square root of brain volume; Braintenberg, 2001; Wang, 2008). Then $D = k_1R$, $B = k_2R$ and $L = k_3R$, with k_1, k_2, k_3 being arbitrary constants. This leads to time delays and FA values which are independent of R, i.e. $FA = \Phi\ \ Nk_2R/k_1R = cons$ and $t = L/kD = k_2R/k\ \ k_1R = cons$. This suggests that only those changes in the microstructural neuroanatomical parameter not linearly proportional related to head size variations lead to variations in FA, time delay or connectivity.

References

Andersen, P., Andersson, S.A., 1968. Physiological Basis Of The Alpha Rhythm. Appleton-Century-Crofts, New York.
Anderson, J., Hutton, C., Ashburner, J., Turner, R, Friston, K., 2001. Modelling geometric deformations in EPI time series. NeuroImage 13, 903–919.
Ashburner, J., Friston, K.J., 1999. Nonlinear spatial normalization using basis functions. Hum. Brain Mapp. 7, 254–266.
Ashtari, M., Cervellione, K.L., Hasan, K.M., Wu, J., McIlree, C., Kester, H., Ardekani, B.A., Roofeh, D., Szeszko, P.R., Kumra, S., 2007. White matter development during late adolescence in healthy males: a cross-sectional diffusion tensor imaging study. NeuroImage 35, 501–510.
Aurlien, H., Gjerde, I.O., Aarseth, J.H., Eldoen, G., Karlsen, B., Skeidsvoll, H., Gilhus, N.E., 2004. EEG background activity described by a large computerized database. Clin. Neurophysiol. 115, 665–673.
Barazany, D., Basser, P.J., Assaf, Y., 2009. In vivo measurement of axon diameter distribution in the corpus callosum of rat brain. Brain 132, 1210–1220.
Beaulieu, C., 2002. The basis of anisotropic water diffusion in the nervous system—a technical review. NMR Biomed. 15, 435–455.
Bloom, J.S., Hynd, G.W., 2008. The role of the corpus callosum in interhemispheric transfer of information: excitation or inhibition? Neuropsychol. Rev. 15, 59–71.
Bollimunta, A., Chen, Y.H., Schroeder, C.E., Ding, M., 2008. Neuronal mechanisms of cortical alpha oscillations in awake-behaving macaques. J. Neurosci. 28, 9976–9988.
Braintenberg, V., 2001. Brain size and number of neurons: an exercise in synthetic neuroanatomy. J. Computat. Neurosci. 10, 71–77.
Buchel, C., Raedler, T., Sommer, M., Sach, M., Weiller, C., Koch, M.A., 2004. White matter asymmetry in the human brain: a diffusion tensor MRI study. Cereb. Cortex 14, 945–951.
Burkitt, G.R., Silberstein, R.B., Cadusch, P.J., Wood, A.W., 2000. The steady-state visually evoked potential and travelling waves. Clin. Neurophysiol. 111, 246–258.
Camara, E., Bodammer, N., Rodriguez-Fornells, A., Tempelmann, C., 2007. Age-related water diffusion changes in human brain: a voxel-based approach. NeuroImage 34, 1588–1599.
Cantero, J.L., Atienza, M., Salas, R.M., Gomez, C.M., 1999. Alpha EEG coherence in different brain states: an electrophysiological index of the arousal level in human subjects. Neurosci. Lett. 271, 167–170.
Chen, X.Y., Jonathan, S.C., Jonathan, R.W., 1992. Constancy of motor axon conduction time during growth in rats. Exp. Brain Res. 90, 343–345.
Connors, B.W., Amitai, Y., 1997. Making waves in the neocortex. Neuron 18, 347–349.
Courchesne, E., Chisum, H.J., Townsend, J., Cowles, A., Covington, J., Egaas, B., Harwood, M., Hinds, S., Press, G.A., 2000. Normal brain development and aging: quantitative analysis at in vivo MR imaging in healthy volunteers. Radiology 216, 672–682.
David, O., Friston, K.J., 2003. A neural mass model for MEG/EEG: coupling and neuronal dynamics. NeuroImage 20, 1743–1755.
De Bellis, M.D., Keshavan, M.S., Beers, S.R., Hall, J., Frustaci, K., Masalehdan, A., Noll, J., Boring, A.M., 2001. Sex differences in brain maturation during childhood and adolescence. Cereb. Cortex 11, 552–557.
Deutsch, G.K., Dougherty, R.F., Bammer, R., Siok, W.T., Gabrieli, J.D.E., Wandell, B., 2005. Children's reading performance is correlated with white matter structure measured by diffusion tensor imaging. Cortex 41, 354–363.
DuMouchel, W.H., O'Brien F.L., 1989. Integrating a Robust Option into a Multiple Regression Computing Environment.
Eyre, J.A., Miller, S., Ramesh, V., 1991. Constancy of central conduction delays during development in man: investigation of motor and somatosensory pathways. J. Physiol. 1991, 441–452.
Flint, A.C., Connors, B.W., 1996. Two types of network oscillations in neocortex mediated by distinct glutamate receptor subtypes and neuronal populations. J. Neurophysiol. 75, 951–956.
Galán, L., Biscay, R., Valdés, P., Neira, L., Virués, T., 1994. Multivariate statistical brain electromagnetic mapping. Brain Topogr. 7, 17–28.
Giorgio, A., Watkins, K.E., Douaud, G., James, A.C., James, S., De Stefano, N., Matthews, P.M., Smith, S.M., Johansen-Berg, H., 2008. Changes in white matter microstructure during adolescence. NeuroImage 39, 52–61.
Goldman, L., Albus, J.S., 1968. Computation of impulse conduction in myelinated fibers; theoretical basis of the velocity-diameter relation. Biophys. J. 8, 596–607.
Grimbert, F., Faugeras, O., 2006. Bifurcation analysis of Jansen's neural mass model. Neural Computation 18, 3052–3068.
Gustafsson, F., 1996. Determining the initial states in forward-backward filtering. IEEE Trans. Signal Process. 44, 988–992.
Hsu, J.L., Leemans, A., Bai, C.H., Lee, C.H., Tsai, Y.F., Chiu, H.C., Chen, W.H., 2008. Gender differences and age-related white matter changes of the human brain: a diffusion tensor imaging study. NeuroImage 39, 566–577.
Hua, K., Zhang, J., Wakana, S., Jiang, H., Li, X., Reich, D.S., Calabresi, P.A., Pekar, J.J., van Zijl, P.C.M., Mori, S., 2008. Tract probability maps in stereotaxic spaces: analyses of white matter anatomy and tract-specific quantification. NeuroImage 39, 336–347.
Hughes, J.R., Ikram, A., Fino, J.J., 1995. Characteristics of traveling waves under various conditions. Clin. Electroencephalogr. 26, 7–22.
Hughes, J.R., Kuruvilla, A., Kino, J.J., 1992. Topographic analysis of visual evoked potentials from flash and pattern reversal stimuli: evidence for "traveling waves". Brain Topogr. 4, 215–228.
Hursh, J.B., 1939a. Conduction velocity and diameter of nerve fibers. Am. J. Physiol. 127, 131–139.
Hursh, J.B., 1939b. The properties of growing nerve fibers. Am. J. Physiol. 127, 140–153.
Hwang, S.N., Chin, C., Wehrli, F.W., Hackney, D.B., 2003. An image-based finite difference model for simulating restricted diffusion. Magn. Reson. Med. 50, 373–382.
Iturria-Medina, Y., Canales-Rodriguez, E.J., Melie-Garcia, L., Valdes-Hernandez, P.A., Martinez-Montes, E., eman-Gomez, Y., Sanchez-Bornot, J.M., 2007. Characterizing brain anatomical connections using diffusion weighted MRI and graph theory. NeuroImage 36, 645–660.

Please cite this article as: Valdés-Hernández, P.A., et al., White matter architecture rather than cortical surface area correlates with the EEG alpha rhythm, NeuroImage (2009), doi:10.1016/j.neuroimage.2009.10.030

Izhikevich, E.M., Edelman, G.M., 2008. Large-scale model of mammalian thalamocortical systems. Proc. Natl. Acad. Sci. U. S. A. 105, 3593–3598.

Jahnsen, H., Llinas, R., 1984. Electrophysiological properties of guinea-pig thalamic neurons—an in vitro study. J. Physiol. London 349 205-&.

Jansen, B.H., Rit, V.G., 1995. Electroencephalogram and visual-evoked potential generation in a mathematical-model of coupled cortical columns. Biological Cybernetics 73, 357–366.

Jansen, B.H., Zouridakis, G., Brandt, M.E., 1993. A neurophysiologically-based mathematical-model of flash visual evoked-Potentials. Biol. Cybern. 68, 275–283.

Jirsa, V.K., 2009. Neural field dynamics with local and global connectivity and time delay. Philos. Trans. R. Soc. A-Math. Phys. Eng. Sci. 367, 1131–1143.

Jirsa, V.K., Haken, H, 1997. A derivation of a macroscopic field theory of the brain from the quasi-microscopic neural dynamics. Physica D 99, 503.

Kim, J.S., Singh, V., Lee, J.K., Lerch, J., Ad-Dab'bagh, Y., MacDonald, D., Lee, J.M., Kim, S.I., Evans, A.C., 2005. Automated 3-D extraction and evaluation of the inner and outer cortical surfaces using a Laplacian map and partial volume effect classification. NeuroImage 27, 210–221.

Le Bihan, D., 2007. The 'wet mind': water and functional neuroimaging. Phys. Med. Biol. 52, R57–R90.

Le Bihan, D., van Zijl, P., 2002. From the diffusion coefficient to the diffusion tensor. NMR Biomed. 15, 431–434.

Liley, D.T.J., Alexander, D.M., Wright, J.J., Aldous, M.D., 1999. Alpha rhythm emerges from large-scale networks of realistically coupled multicompartmental model cortical neurons. Netw.-Comput. Neural Syst. 10, 79–92.

Liley, D.T.J., Cadusch, P.J., Dafilis, M.P., 2002. A spatially continuous mean field theory of electrocortical activity. Netw.-Comput. Neural Syst. 13, 67–113.

Lopes da Silva, F., 1991. Neural mechanisms underlying brain waves: from neural membranes to networks. Electroencephalogr. Clin. Neurophysiol. 79, 81–93.

Lopes da Silva, F.H., Hoeks, A., Smits, H., Zetterberg, L.H., 1974. Model of brain rhythmic activity. The alpha-rhythm of the thalamus. Kybernetik 15, 27–37.

Lopes da Silva, F.H., Storm van Leeuwen, W., 1978. The cortical alpha rhythm in dog: the depth and surface profile of phase. In: Brazier, M.A.B., Petsche, H. (Eds.), Architectonics of the Cerebral Cortex. Raven Press, New York, pp. 319–333.

Lopes da Silva, F.H., Vos, J.E., Mooibroek, J., Van Rotterdam, A., 1980. Relative contributions of intracortical and thalamo-cortical processes in the generation of alpha rhythms, revealed by partial coherence analysis. Electroencephalogr. Clin. Neurophysiol. 50, 456.

Madden, D.J., Whiting, W.L., Huettel, S.A., White, L.E., MacFall, J.R., Provenzale, J.M., 2004. Diffusion tensor imaging of adult age differences in cerebral white matter: relation to response time. NeuroImage 21, 1174–1181.

Mädler, B., Drabycz, S.A., Kolin, S.H., Whittall, K.P., MacKay, A., 2008. Is diffusion anisotropy an accurate monitor of myelination? Correlation of multicomponent T2 relaxation and diffusion tensor anisotropy in human brain. Magn. Reson. Imaging 26, 874–888.

Mangin, J.F., Riviere, D., Cachia, A., Duchesnay, E., Cointepas, Y., Papadopoulos-Orfanos, D., Scifo, P., Ochiai, T., Brunelle, F., Regis, J., 2004. A framework to study the cortical folding patterns. NeuroImage 23, S129–S138.

Manjarrez, E., Vazquez, M., Flores, A., 2007. Computing the center of mass for traveling alpha waves in the human brain. Brain Res. 1145, 239–247.

Massimini, M., Huber, R., Ferrarelli, F., Hill, S., Tononi, G., 2004. The sleep slow oscillation as a traveling wave. J. Neurosci. 24, 6862–6870.

Mazziotta, J., Toga, A., Evans, A., Fox, P., Lancaster, J., Zilles, K., Woods, R., Paus, T., Simpson, G., Pike, B., Holmes, C., Collins, L., Thompson, P., MacDonald, D., Iacoboni, M., Schormann, T., Amunts, K., Palomero-Gallagher, N., Geyer, S., Parsons, L., Narr, K., Kabani, N., Le Goualher, G., Boomsma, D., Cannon, T., Kawashima, R., Mazoyer, B., 2001. A probabilistic atlas and reference system for the human brain: International Consortium for Brain Mapping (ICBM). Philos. Trans. R. Soc. Lond., B Biol. Sci. 356, 1293–1322.

Mori, S., Oishi, K., Jiang, H.Y., Jiang, L., Li, X., Akhter, K., Hua, K.G., Faria, A.V., Mahmood, A., Woods, R., Toga, A.W., Pike, G.B., Neto, P.R., Evans, A., Zhang, J.Y., Huang, H., Miller, M.I., Zijl, P., Mazziotta, J., 2008. Stereotaxic white matter atlas based on diffusion tensor imaging in an ICBM template. NeuroImage 40, 570–582.

Moseley, M., 2002b. Diffusion tensor imaging and aging—a review. NMR Biomed. 15, 553–560.

Moseley, M., 2002a. Diffusion tensor imaging and aging—a review. NMR Biomed. 15, 553–560.

Niedermeyer, E., Lopes da Silva, F.H., 2004. Electroencephalography, 5 ed. Limppicott Williams & Wilkins, Limppicott Williams & Wilkins.

Nunez, P.L., Cutillo, B.A., Gevins, A.S., 1995. Neocortical Dynamics and Human EEG Rhythms. Oxford University Press.

Nunez, P.L., Reid, L., Bickford, R.G., 1978. Relationship of head size to alpha frequency with implications to a brain wave model. Electroencephalogr. Clin. Neurophysiol. 44, 344–352.

Nunez, P.L., Srinivasan, R., 2006. A theoretical basis for standing and traveling brain waves measured with human EEG with implications for an integrated consciousness. Clin. Neurophysiol. 117, 2424–2435.

Nunez, P.L., Wingeier, B.M., Silberstein, R.B., 2001. Spatial-temporal structures of human alpha rhythms: theory, microcurrent sources, multiscale measurements, and global binding of local networks. Hum. Brain Mapp. 13, 125–164.

Oppenheim, A.V., Schafer, R.W., 1989. Discrete-Time Signal Processing. Prentice-Hall, pp. 311–312.

Pabitra, S., Basser, P., 2005. A model for diffusion in white matter in the brain. Biophys. J. 89, 2927–2938.

Paparoditis, E., Politis, D.N., 2005. Bootstrap hypothesis testing in regression models. Stat. Probab. Lett. 74, 356–365.

Pfefferbaum, A., Sullivan, E.V., Hedehus, M., Lim, K.O., Adalsteinsson, E., Moseley, M., 2000. Age-related decline in brain white matter anisotropy measured with spatially corrected echo-planar diffusion tensor imaging. Magn. Reson. Med. 44, 259–268.

Posthuma, D., Neale, M.C., Boomsma, D.I., de Geus, E.J.C., 2001. Are smarter brains running faster? Heritability of alpha peak frequency, IQ, and their interrelation. Behav. Genet. 31, 567–579.

Rennie, C.J., Robinson, P.A., Wright, J.J., 1999. Effects of local feedback on dispersion of electrical waves in the cerebral cortex. Phys. Rev. E 59, 3320–3329.

Reutskiy, S., Rossoni, E., Tirozzi, B., 2003. Conduction in bundles of demyelinated nerve fibers: computer simulation. Biol. Cybern. 89, 439–448.

Robbins, S.M., 2003. Anatomical Standardization of the Human Brain in Euclidean 3-Space and on the Cortical 2-Manifold. School of Computer Science. McGill University, Montreal.

Roberts, J.A., Robinson, P.A., 2008. Modeling distributed axonal delays in mean-field brain dynamics. Phys. Rev. E 78.

Robinson, P.A., Rennie, C.J., Wright, J.J., 1997. Propagation and stability of waves of electrical activity in the cerebral cortex. Phys. Rev. e 56, 826–840.

Robinson, P.A., Rennie, C.J., Wright, J.J., Bourke, P.D., 1998. Steady states and global dynamics of electrical activity in the cerebral cortex. Phys. Rev. E 58, 3557–3571.

Robinson, P.A., Loxley, P.N., O'Connor, S.C., Rennie, C.J., 2001a. Modal analysis of corticothalamic dynamics, electroencephalographic spectra, and evoked potentials. Phys. Rev. E 6304.

Robinson, P.A., Loxley, P.N., O'Connor, S.C., Rennie, C.J., 2001b. Modal analysis of corticothalamic dynamics, electroencephalographic spectra, and evoked potentials. Phys. Rev. E 6304.

Robinson, P.A., Rennie, C.J., Wright, J.J., Bahramali, H., Gordon, E., Rowe, D.L., 2001c. Prediction of electroencephalographic spectra from neurophysiology. Phys. Rev. E 6302 art-021903.

Robinson, P.A., Rennie, C.J., Rowe, D., O'Connor, S.C., Wright, J.J., Gordon, E., Whitehouse, R.W., 2003a. Neurophysical modeling of brain dynamics. Neuropsychopharmacology 28, S74–S79.

Robinson, P.A., Whitehouse, R.W., Rennie, C.J., 2003b. Nonuniform corticothalamic continuum model of electroencephalographic spectra with application to split-alpha peaks. Phys. Rev. E 68.

Rushton, W.A.H., 1951. A theory of the effects of fibre size in medullated nerve. J. Physiol. 115, 101–122.

Sabah, N.H., 2000. Aspects of nerve conduction. IEEE Eng. Med. Biol. Mag. 19, 111–118.

Salami, M., Itami, C., Tsumoto, T., Kimura, F., 2003. Change of conduction velocity by regional myelination yields constant latency irrespective of distance between thalamus and cortex. Proc. Natl. Acad. Sci. U. S. A. 100, 6174–6179.

Salat, D.H., Tuch, D.S., Greve, D.N., van der Kouwe, A.J.W., Hevelone, N.D., Zaleta, A.K., Rosen, B.R., Fischl, B., Corkin, S., Rosas, H.D., Dale, A.M., 2005. Age-related alterations in white matter microstructure measured by diffusion tensor imaging. Neurobiol. Aging 26, 1215–1227.

Schneiderman, J.S., Buchsbaum, M.S., Haznedar, M.M., Hazlett, E.A., Brickman, A.M., Shihabuddin, L., Brand, J.G., Torosjan, Y., Newmark, R.E., Tang, C., Aronowitz, J., Paul-Odouard, R., Byne, W., Hof, P.R., 2007. Diffusion tensor anisotropy in adolescents and adults. Neuropsychobiology 55, 96–111.

Smith, S., 2002. Fast robust automated brain extraction. Hum. Brain Mapp. 17, 143–155.

Sotero, R.C., Trujillo-Barreto, N.J., Iturria-Medina, Y., Carbonell, F., Jimenez, J.C., 2007. Realistically coupled neural mass models can generate EEG rhythms. Neural Comput. 19, 478–512.

Steriade, M., Gloor, P., Llinas, R., Lopes da Silva, F.H., Mesulam, M.M., 1990. Basic mechanisms of cerebral rhythmic activities. Electroencephalogr. Clin. Neurophysiol. 76, 508.

Stufflebeam, S.M., Witzel, T., Mikulski, S., Hamalainen, M.S., Temereanca, S., Barton, J.S. S., Tuch, D.S., Manoach, D.S., 2008. A Non-Invasive Method to Relate the Timing of Neural Activity to White Matter Microstructural Integrity.

Sullivan, E.V., Pfefferbaum, A., 2006. Diffusion tensor imaging and aging. Neurosci. Biobehav. Rev. 30, 749–761.

Szeszko, P.R., Vogel, J., Ashtari, M., Malhotra, A.K., Bates, J., Kane, J.M., Bilder, R.M., Frevert, T., Lim, K., 2003. Sex differences in frontal lobe white matter microstructure: a DTI study. NeuroReport 14, 2469–2473.

Thirion, JP., 1998. Image matching as a diffusion process: an analogy with Maxwell's demons. Med. Image Anal. 2, 243–260.

Udulag, K., Evans, A.C., Della-Maggiore, V., Murer, G., Amaro, E., Sierra, O., Valdés-Hernández, P.A., Medina, V., Valdés-Sosa, P.A., 2008. Latin American brain mapping network. Int. J. Bioelectromagn. 10, 281–299.

Valdés, P., Virués, T., Szava, S., Galán, L., Biscay, R., 1990. High resolution spectral EEG norms topography. Brain Topogr. 3, 281–282.

Valdes, P., Valdes, M., Carballo, J.A., Álvarez, A., Diaz, G.F., Biscay, R., Perez, M.C., Szava, S., Virues, T., Quesada, M.E., 1992. QEEG in a public health system. Brain Topogr. 4, 259–266.

Valdes-Sosa, P.A., Sanchez-Bornot, J.M., Sotero, R.C., Iturria-Medina, Y., Alemán-Gómez, Y., Bosch-Bayard, J., Carbonell, F., Ozaki, T., in press. Model driven EEG/fMRI fusion of brain oscillations. Human Brain Mapping, (in press) doi:10.1002/hbm.20704. Q1

Van Rotterdam, A., Dasilva, F.H.L., Vandenende, J., Viergever, M.A., Hermans, A.J., 1982. A model of the spatial-temporal characteristics of the alpha-rhythm. Bull. Math. Biol. 44, 283–305.

Vega-Hernandez, M., Martinez-Montes, E., Sanchez-Bornot, JM, Lage-Castellanos, A., Valdes-Sosa, P.A., 2008. Penalized least squares methods for solving the EEG Inverse problem. Statistica Sinica 18, 1535–1551.

Wang, S., 2008. Functional tradeoffs in axonal scaling: implications for brain function. Brain Behav. Evol. 72, 159–167.

Waxman, S.G., 1980. Determinants of conduction velocity in myelinated nerve fibers. Muscle Nerve 3, 141–150.

Please cite this article as: Valdés-Hernández, P.A., et al., White matter architecture rather than cortical surface area correlates with the EEG alpha rhythm, NeuroImage (2009), doi:10.1016/j.neuroimage.2009.10.030

Whitford, T.J., Rennie, C.J., Grieve, S.M., Clark, C.R., Gordon, E., Williams, L.M., 2007. Brain maturation in adolescence: concurrent changes in neuroanatomy and neurophysiology. Hum. Brain Mapp. 28, 228–237.

Wingeier, B.M., Nunez, P.L., Silberstein, R.B., 2001. Spherical harmonic decomposition applied to spatial-temporal analysis of human high-density electroencephalogram. Phys. Rev. E 6405.

Wright, J.J., Liley, D.T.J., 1995. Simulation of electrocortical waves. Biol. Cybern. 72, 347–356.

Wright, J.J., Liley, D.T.J., 1996. Dynamics of the brain at global and microscopic scales: neural networks and the EEG. Behav. Brain Sci. 19 285-&.

Wright, J.J., Robinson, P.A., Rennie, C.J., Cordon, E., Bourke, P.D., Chapman, C.L., Hawthorn, N., Lees, G.J., Alexander, D., 2001. Toward an integrated continuum model of cerebral dynamics: the cerebral rhythms, synchronous oscillation and cortical stability. Biosystems 63, 71–88.

Wu, J.Y., Huang, X., Zhang, C., 2008. Propagating waves of activity in the neocortex: what they are, what they do. Neuroscientist 14, 487–502.

Please cite this article as: Valdés-Hernández, P.A., et al., White matter architecture rather than cortical surface area correlates with the EEG alpha rhythm, NeuroImage (2009), doi:10.1016/j.neuroimage.2009.10.030